Experimental and numerical investigations of CPT end resistance at variable penetration rates in mixed soils

Aflizal Arafianto[1#], *Yishan* Tian[1], *Barry* Lehane[1], *Yusuke* Suzuki[2], and *David* Reid[1]

[1]*The University of Western Australia, Department of Civil, Environmental and Mining Engineering, 35 Stirling Hwy, Crawley, WA 6009, Australia*
[2]*Norwegian Geotechnical Institute, P.O. Box. 3930 Ullevål Stadion, N-0806 Oslo, Norway*
[#]*Corresponding author: aflizal.arafianto@research.uwa.edu.au*

ABSTRACT

This paper investigated cone penetration test end resistance under various drainage conditions in mixed soils through numerical simulations and piezocone experiments in laboratory testing chambers. The soil samples used in the laboratory tests contained various proportions of kaolin, silt, and sand. The piezocone tests were performed using a 10 mm diameter cone in consolidated soil samples. The measured variations of cone resistance and pore pressure at cone velocities varying from 0.005 mm/s to 30 mm/s are presented, which covered the full range from drained to undrained conditions. The cone resistance was evaluated using the spherical cavity expansion limit pressure predicted in Finite Element (FE) analyses that employed the NorSand (NS) constitutive model. The experimental and numerical findings allow assessment of the suitability of the normalised velocity (V) term, proposed by others, to unify cone resistances measured at variable rates.

Keywords: Cone penetration test; rate effect; drainage condition; spherical cavity expansion; mixed soils; NorSand constitutive model

1. Introduction

The end resistance of a penetrometer depends on the penetrometer velocity, and this dependence arises primarily because the level of drainage possible around a cone reduces with increasing velocity. Jaeger et al. (2010), for example, found that the cone resistance at slow drained rates in a particular soil was more than 15 times greater than the resistance at fast undrained rates.

This paper investigates the potential of a simple numerical method to provide reasonable predictions of the rate dependence of cone resistance measured in Cone Penetration Tests (CPTs). The cone resistance (q_t) is estimated from the spherical cavity expansion limit pressure (p_{limit}) computed using the finite element (FE) method and the NorSand (NS) constitutive soil model (Jefferies and Been 2015; Jefferies and Shuttle 2005). The FE modelling approach and analysis steps are based on Suzuki and Lehane (2015a), who employed a relationship between q_t and p_{limit} incorporating the pore pressure term and between cone velocity and rate of cavity expansion to allow estimation of q_t values at various cone velocities. The FE results are compared with experimental data in two soil mixtures with varying clay, silt, and sand proportions to evaluate the potential of the NorSand model for this application. A series of parametric analyses is also presented to examine the effects of stiffness, strength, consolidation characteristics and initial state parameter (ψ_0) on penetration resistance at different penetration rates. These analyses assist assessment of a normalised velocity (V) term to unify the penetration resistance vs velocity characteristic for a range of soil types.

2. Soil properties

Two soil mixtures are used in this study: Sand-Clay-Silt (SCS) and Sand-Clay (25% Kaolin), both of which have been the subject of separate characterisation studies at The University of Western Australia (UWA). The SCS sample has proportions (by dry mass) of 31% UWA sand, 43% silt, and 26% Kaolin clay. This mixture was made with the same material type and proportion as the "UT" sample mentioned in Reid and Fourie (2016). The second soil mixture, as the name suggests, comprises 25% Kaolin and 75% sand; this mixture was studied by Suzuki (2015) specifically to investigate the effect of penetration rate on the CPT end resistance. Table 1 lists the basic material properties of the two soil types.

Table 1. Index properties summary (Reid and Fourie 2016; Suzuki 2015)

Property	SCS	25% Kaolin
Specific gravity, G_s	2.62	2.638
Liquid limit, *LL* (%)	24	20
Plastic limit, *PL* (%)	15	14
Plasticity index, *PI* (%)	9	6
Coefficient of consolidation, c_v (m^2/year) at σ_v' = 55 kPa	12	22

3. Physical experiments

CPTs at various penetration rates in the SCS and 25% Kaolin samples were conducted in laboratory pressure chambers. The testing equipment and procedures for the SCS sample are described below, while full details concerning the experiments in 25% Kaolin are provided by Suzuki (2015) and Suzuki and Lehane (2015b). In

principle, the two testing methods and the CPT probes used were very similar.

The SCS sample was prepared at 122% water content, thoroughly mixed until the desired consistency was achieved, and finally transferred carefully into the testing chamber. A hydraulic press with precision load control was used throughout the consolidation process, from an initial vertical stress of 0.5 kPa to the final stress of 55 kPa.

Upon reaching the target stress level (55 kPa), the chamber was transferred to a weight-loaded lever arm system where the CPT was conducted (Fig. 1). The vertical stress on the sample was maintained at 55 kPa during the CPTs, which were conducted via circular openings in the top plate. The actuator, fixed to the chamber flange, pushed a 10-mm diameter cone into the sample at various constant velocities (v=0.005, 0.05, 0.15, 0.5, 2, and 30 mm/s). The penetrometer had a built-in load cell at the tip and a pressure sensor at the cone shoulder to measure tip resistance (q_t) and pore pressure (u_2), which is transmitted to a logger via a cable connection. Cone resistance and pore pressure profiles in Fig. 2 illustrate the effects of variable penetration rate testing on penetration resistance and induced pore pressure.

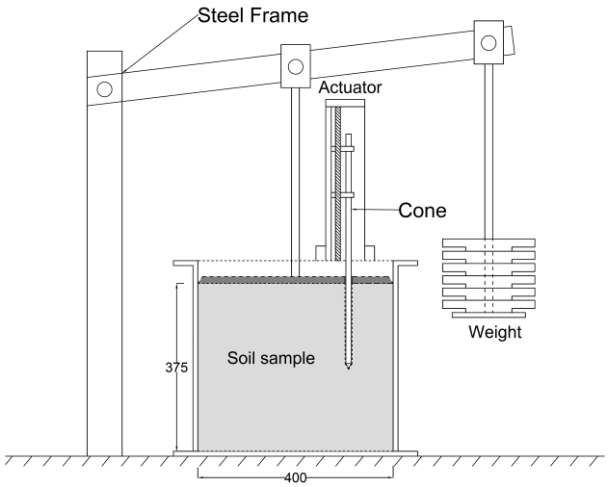

Figure 1. Schematic of laboratory pressure chamber test

A cone dissipation test was also performed at the end of the undrained installation (v=30 mm/s), which indicated a coefficient of horizontal consolidation (c_h) value of about 20 m^2/year.

The effect of the proximity of chamber boundaries on recorded data has been investigated by Bolton et al. (1999), who suggest a minimum value of d_c/d_{50} equal to 20, where d_c is cone diameter, and d_{50} is mean grain size; this criterion was satisfied for the CPTs in both the SCS and 25% Kaolin soils. The testing locations were at least ten cone diameters (10 d_c) away from the chamber walls, as recommended by Bolton et al. (1999).

To construct the cone resistance vs velocity characteristic, for consistency, only piezocone measurements from between 200 and 260 mm are plotted. However, measurements plotted at penetration rates of 0.15 mm/s and 30 mm/s were from the depth intervals 100 to 150 mm and 15 to 60 mm, respectively.

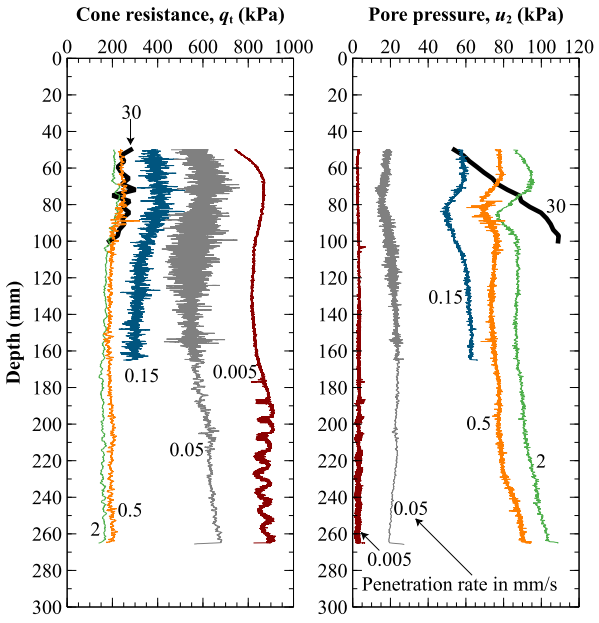

Figure 2. CPT profiles at variable penetration rates in SCS sample

4. Element testing

Routine laboratory tests (i.e., triaxial compression and simple shear) are commonly used to derive NorSand parameters. In this study, isotropically consolidated undrained (CIU) triaxial test measurements reported by Reid and Fourie (2016) were utilised to calibrate NorSand parameters for the SCS mixture, while undrained simple shear test data from Suzuki (2015) were employed for the 25% Kaolin. The sample preparation method and testing procedure are explained in detail in the respective references.

The "Sand" in the NorSand model's name emphasizes its ability to properly represent dilation found in denser soils. NorSand, however, is not exclusively restricted to sands, and its most prominent applications have been for intermediate soils (e.g., clayey silts or silty sands). Specific features in this constitutive model relevant to this study are as follows:

- Inclusion of state parameter (ψ) as a critical controlling variable to capture a full range of soil behaviour from contractant loose soils to dilative dense soils.
- An option for cap softening in the hardening law is available by employing the softening flag (S) parameter. Shuttle et al. (2022) stated that this parameter is an accelerator for when excess pore pressure is changing rapidly.

Parameter calibration was performed on element test modules using the PLAXIS (Bentley Systems Inc., 2022) SoilTest feature. The calibration process started with inputting parameter values derived from previous laboratory assessments for a given estimate of the initial state parameter (ψ_0). This process was followed by trial and error until predicted and measured data were sufficiently matched. The derived parameters for both samples are listed in Table 2.

Table 2. Calibrated NorSand parameters for SCS and 25% Kaolin mixtures

Parameter Definition		SCS	25% Kaolin
Reference value of the shear modulus at the reference pressure (kPa)	G_{ref}	45000	12000
Reference mean pressure (kPa)	p_{ref}	245	100
Exponent of the power-law elasticity (-)	n_G	1	1
Poisson's ratio (-)	ν	0.2	0.2
Void ratio corresponding to a mean pressure equal to 1 kPa (-)	Γ	0.59	0.55
Slope of the critical state (e-$ln(p)$) (-)	λ_e	0.016	0.029
Friction ratio at critical state in triaxial conditions (-)	M_{tc}	1.30	1.37
Material parameter controlling the maximum stress ratio as a function of the minimum dilatancy (-)	N	0.1	0.2
Material parameter which governs the slope of the minimum dilatancy as a function of the state parameter (-)	χ_{tc}	9	20
Hardening parameter (-)	H_0	120	500
Hardening parameter (-)	H_ψ	0	0
Over-consolidation ratio	R	1.05	1
Softening flag (-)*	S	1	1
Initial value of the state parameter (-)	ψ_0	0.01	0.03
Horizontal permeability (m/s)	k_x	8.4×10^{-9}	1×10^{-8}
Vertical permeability** (m/s)	k_y	4.2×10^{-9}	5×10^{-9}

*S=1 was inputted only during undrained penetration (i.e., v_{cone} > 1 mm/s).
**Permeability values are at an initial void ratio (e_0) of 0.44 and 0.50 for SCS and 25% Kaolin, respectively.

The parameter M_{tc} is a function of the constant volume friction angle (ϕ_{cv}) given by the Mohr-Coulomb expression as:

$$M_{tc} = \frac{6\sin(\phi_{cv})}{3-\sin(\phi_{cv})} \quad (1)$$

The M_{tc} values input to PLAXIS SoilTest are consistent with the ϕ_{cv} reported by Reid and Fourie (2016) and Suzuki (2015). The PLAXIS SoilTest calculations adopted the Extended Dafalias option by inputting the $M_{tc} > 0$. A full description of this procedure is provided in the PLAXIS User Defined Soil Models (UDSM) - NorSand manual (Bentley Systems, Inc., 2022).

Vertical permeability values (at 55 kPa of vertical effective stress) were determined based on laboratory tests performed by Suzuki (2015) and Reid and Fourie (2016). Horizontal permeability values for both mixtures were assumed to be twice the vertical permeability (k_x=2·k_y). Suzuki (2015) adopted the same assumption for the 25% Kaolin sample.

Fig. 3 and Fig. 4 compare the predicted stress-strain behaviour and stress paths from PLAXIS SoilTest simulations and experimental data. It is seen that the predicted shear strength at the end of the tests is in good agreement with the measurements. The pre-failure response of SCS is well predicted by NorSand, but the peak response for the 25% Kaolin is not captured by the model.

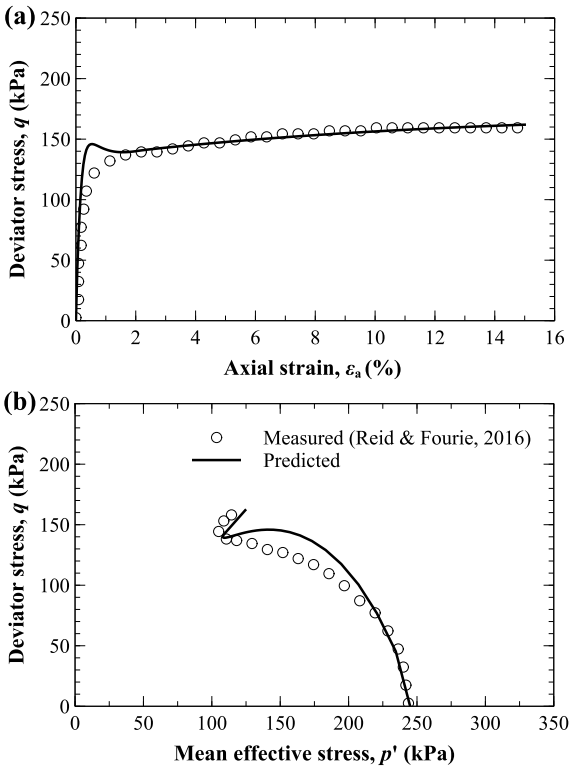

Figure 3. SCS mixture CIU test results and NorSand (NS) model predictions on (a) deviator stress vs axial strain and (b) effective stress path

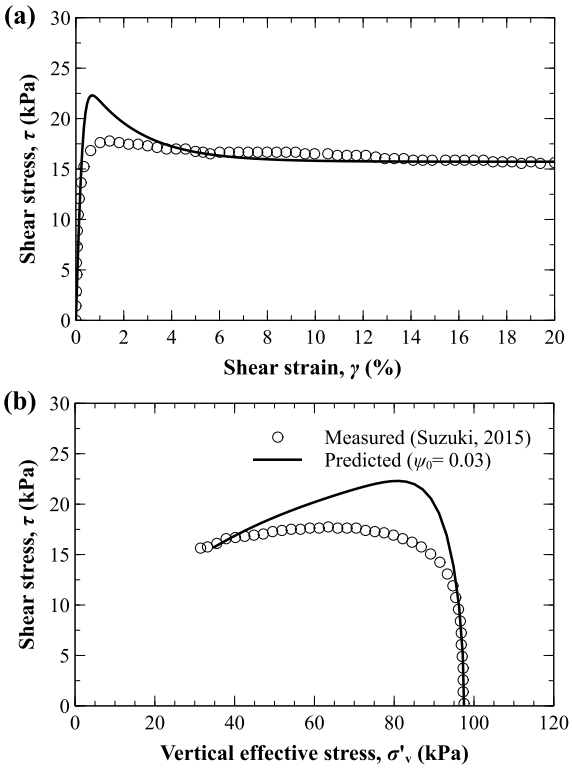

Figure 4. 25% Kaolin mixture simple shear test results (σ_v' = 100 kPa; K_0 = 0.5) and NorSand predictions on (a) shear stress vs shear strain and (b) σ_v' vs τ

5. Numerical analyses

5.1. FE modelling approach and analysis steps

The limit pressure, hence cone resistance, was evaluated by finite element (FE) spherical cavity expansion (SCE) simulations, which have been employed successfully by Suzuki and Lehane (2015a) using PLAXIS 2D and the hardening soil model (Schanz et al. 1999). An axisymmetric model with standard fixities (i.e., horizontally fixed on side boundaries, fully fixed at the bottom boundary, and free at the model's top) was adopted. As for flow boundaries, the bottom and the top are left open while the sides are closed. Fig. 5 shows the mesh configuration and model dimensions, with a cavity cluster (initial cavity radius a_0 of 2 mm) 240 mm above the bottom boundary line. No boundary effects were indicated with these settings. The cavity cluster is an elastic material with Young's modulus (E) and Poisson's ratio (ν) of 20 MPa and 0.2, respectively. The phreatic level was set at the top boundary line, resulting in a hydrostatic pressure (u_0) of 2.4 kPa.

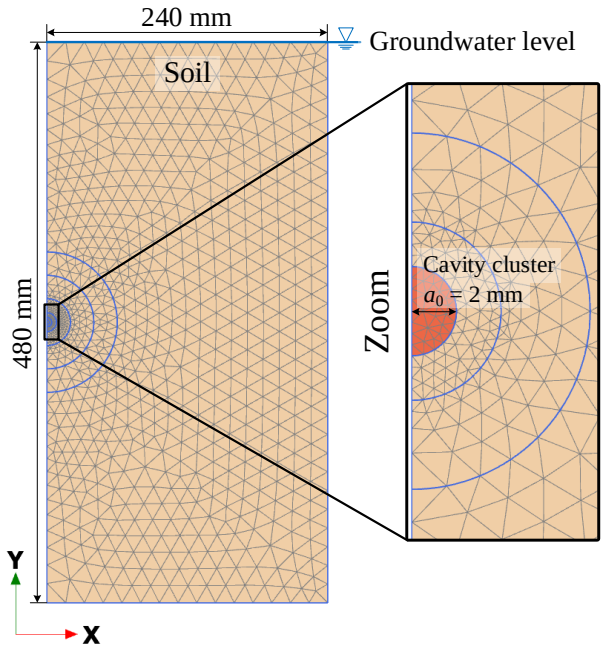

Figure 5. Finite Element (FE) model mesh configuration

A single FE simulation (with a particular cavity expansion velocity) comprises initial stress generation and spherical cavity expansion phases. The initial stresses were defined using the lateral coefficient (K_0) procedure, where in this study, K_0 = 0.5 was assumed for both SCS and 25% Kaolin mixtures. Since the FE model dimensions are relatively small, the inputted soil's unit weight is selected to produce an initial vertical effective stress (σ'_v) of 55 kPa at the centre of the cavity cluster. After initial stresses are generated, a positive volumetric strain is applied to the cavity cluster, enabling the cavity to expand. In PLAXIS, the consolidation calculation type was selected during this phase with an updated mesh and water pressure options (in the deformation control parameters subtree) turned on; detailed explanations of these options are provided in the PLAXIS 2D Reference Manual (Bentley Systems Inc., 2023). These two options are employed to account for the geometry change of the mesh (due to the cavity expansion) on the equilibrium conditions. The time interval input was selected to simulate various expanding velocities, which can later be converted to cone penetration rates.

Lastly, to extract expansion and excess pore pressure outputs, seven stress points and seven displacement nodes next to the cavity cluster were selected; their locations followed the same configuration as Suzuki (2015). Under the "numerical control parameters" setting in the analysis window, the maximum load fraction per step was set to 0.01 to produce more data points for smoother output curves.

5.2. Converting cone resistance (q_t) and penetration rate (v_{cone}) from SCE

A number of workers have examined the relationship between spherical cavity expansion limit pressure (p_{limit}) and cone resistance (q_t) (e.g., Ladanyi and Johnston 1974; Silva 2005; Vesić 1972, 1977; Yasufuku and Hyde 1995). This paper relates q_t with p_{limit} using a relationship employed by Suzuki and Lehane (2015a) based on vertical force equilibrium and pore pressures (u) acting on this face equal to evaluated at the limit pressure:

$$q_t = p_{\text{limit}} + \sqrt{3}(p_{\text{limit}} - u)\tan\delta \qquad (2)$$

where δ is the soil-cone interface friction angle and the effective cohesion (c') of the soil is assumed to be zero. The value of p_{limit} was determined as the averaged maximum principal total stress (σ_1) from previously selected stress points at radial displacements (a) equal to two times the initial radius ($a = 2{\cdot}a_0$). The pore pressure was also taken as an average of seven points next to the cavity wall at this normalised radial displacement (a/a_0). The δ value was assumed to equal the constant volume friction angle (ϕ_{cv}). This assumption has been shown by Silva (2005), Suzuki and Lehane (2015a), and others, to lead to good predictions of cone resistance, acknowledging that the simulation approach is an approximate means of modelling actual cone penetration.

The spherical cavity expansion velocity (v_{CE}) is assumed to be the resultant velocity in a direction normal to the cone face. With a typical cone apex angle of 60° and cone penetration in the vertical direction, the cone velocity (v_{cone}) can be calculated with an equation below:

$$v_{\text{cone}} = \cos 60° \cdot v_{\text{CE}} = \frac{1}{2} \cdot v_{\text{CE}} \qquad (3)$$

Fig. 6 plots the predicted cavity and excess pore pressures against the normalised radial displacement with various cavity expansion velocities for the SCS case. The cavity pressure decreases, and excess pore pressure increases as the v_{CE} increases, showing dependency on the expansion rates. It is evident that fluctuation occurred during the undrained cavity expansion (i.e., in ranges ~4.3 to 130 mm/s), where the softening flag parameter (S) was switched on at these two velocities. A fully drained condition was confirmed at v_{CE} of 0.00043 mm/s, where the generated excess pore pressures at this cavity expansion velocity were zero (or very close to zero).

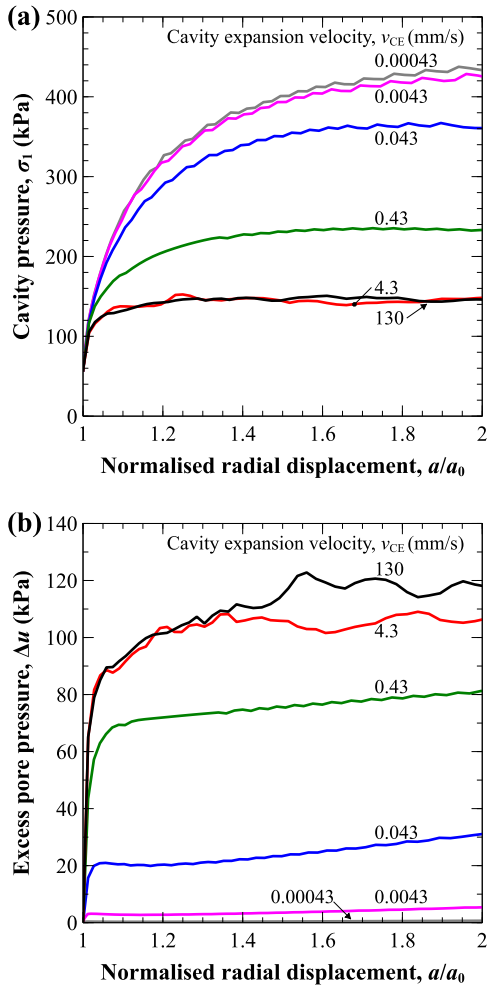

Figure 6. Averaged cavity expansion and excess pore pressure responses with different expansion rates for SCS case

5.3. Comparison with experimental data

Net cone resistance values ($q_{tnet} = q_t - \sigma_{v0}$) predicted from the FE analyses are compared here with experimental data in 25% Kaolin reported in Suzuki (2015) and SCS mixture in this study, shown in Fig. 7. Cone velocities ranging from 0.0002 to 40±20 mm/s (six orders of magnitude) were simulated to cover the full range of measured data to obtain the q_{tnet} vs v_{cone} characteristic for each soil.

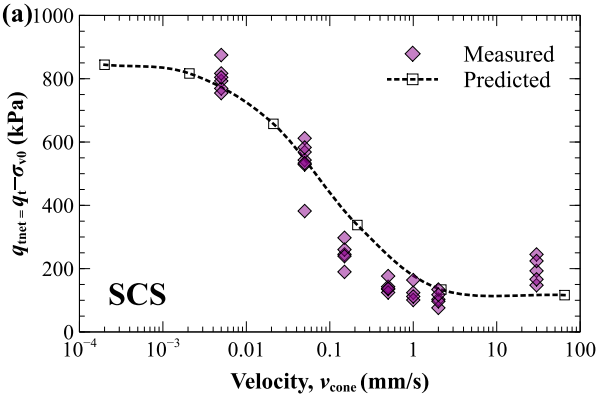

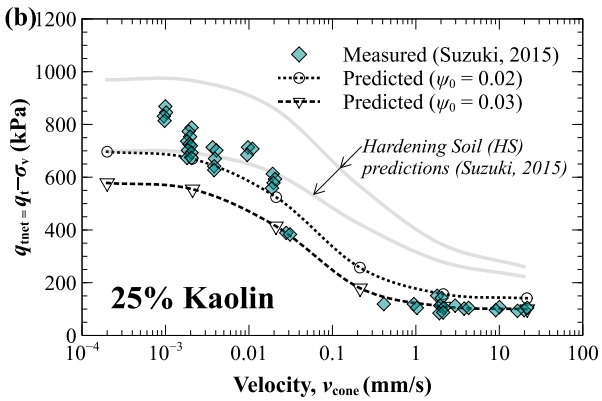

Figure 7. Comparison of FE-predicted net cone resistance and pressure chamber experiment results for (a) SCS and (b) 25% Kaolin

In the SCS mixture, it is evident that a very good agreement between measurements and predictions is obtained over the full velocity range. However, not unsurprisingly, the enhanced resistance due to viscous effects at very high velocities is not captured.

As seen in Fig. 7(b), the computed cone resistances for the 25% Kaolin soil matched the laboratory measurements reasonably well when the initial state parameter (ψ_0) was set to 0.02. The corresponding predictions presented by Suzuki (2015) using the hardening soil (HS) model are also presented in Fig. 7(b) and evidently are not capable of predicting the observed ratio of drained to undrained strengths. The transition velocities between drained and partially drained and between partially drained and undrained conditions for the HS and NorSand predictions are similar.

It is apparent that NorSand's incorporation of the initial state parameter results in better predictions of cone resistances with various penetration rates, even in two different soil mixtures with proportions of sand, silt, and clay. A better understanding of this constitutive model, particularly its implementation to penetration rate effects, is explored through a parametric study in the following section.

5.4. Parametric study

The primary purpose of the parametric study presented in the following is to assess the key parameters influencing the cone resistance vs velocity characteristic. Dienstmann et al. (2018) pointed out that the cone resistance depends primarily on the soil compressibility (λ and κ), shear strength (ϕ') and soil consolidation characteristics (c_h); these findings are consistent with Lehane et al. (2009), Suzuki and Lehane (2015a), and others.

Therefore, a series of analyses (using NorSand for the SCS mixture) presented below examine the effects of stiffness, strength, and permeability values on the cone resistance under different drainage conditions. The effect of the initial state parameter (hence, the current state of the soil) was also carried out to give new insights.

5.4.1. Effect of stiffness (G/p_0')

Three cases examined the effect of soil stiffness in terms of normalised modulus (G/p'_0), where G is the equivalent linear shear modulus of the soil mass and p'_0

is the initial mean effective stress. In NorSand, the shear modulus varies with mean effective stress:

$$G = G_{\text{ref}} \left(\frac{p'}{p'_{\text{ref}}} \right)^{n_G} \quad (4)$$

The stiffness effects were investigated by varying the G_{ref} values (hence, different G values were obtained) and keeping all parameters listed in Table 2 the same (including the K_0 value for initial stress generation). Fig. 8 demonstrates how stiffness affects the magnitude of the net cone resistances and overall backbone curve shape.

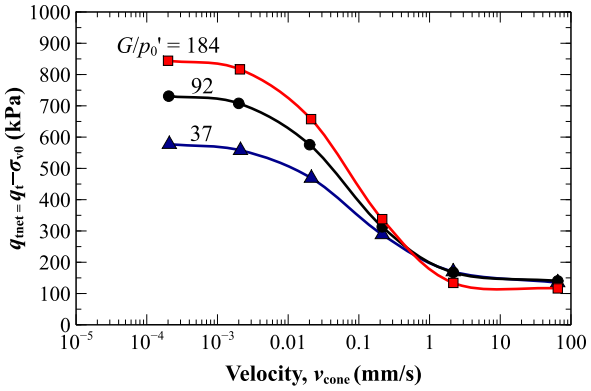

Figure 8. Effect of stiffness on cone resistance dependence on velocity predicted by NorSand

It is seen in Fig. 8 that the undrained cone resistances of soil with the highest stiffness are slightly lower than calculated undrained cone resistances at the other two stiffnesses. This finding differs from that found using the hardening soil (HS) model (Suzuki and Lehane 2015a), which showed that undrained cone resistances increased with the ratio of stiffness to initial mean effective stress.

5.4.2. Effect of strength (M_{tc})

Strength effects were assessed by varying inputted M_{tc} values. Calculated net cone resistance for three different M_{tc} values are shown in Fig. 9.

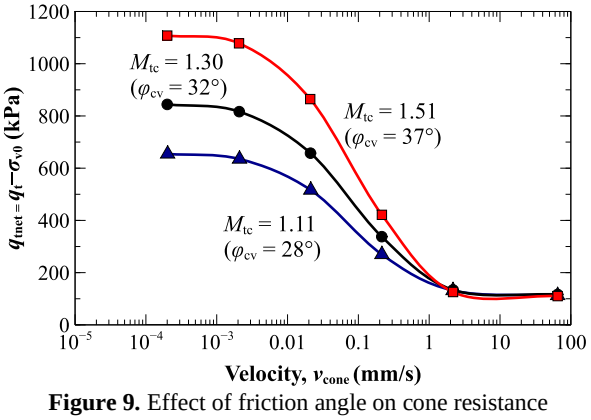

Figure 9. Effect of friction angle on cone resistance dependence on velocity predicted by NorSand

Surprisingly, the undrained cone resistances for all three different M_{tc} values are approximately the same, which is in contrast to the increase in undrained resistance with friction angle found by Suzuki and Lehane (2015a) for the hardening soil model.

5.4.3. Effect of permeability (k)

The effect of permeability was evaluated by increasing the permeability values (horizontal and vertical) 100 times higher than the original values in Table 2. Analyses were performed for anisotropic permeability conditions, where the horizontal permeability is two times faster than in the vertical direction ($k_h = 2 \cdot k_v$). Increasing the permeability shifted the $q_{tnet} - v_{cone}$ curve to the right by two orders of magnitude, as shown in Fig. 10, consistent with Suzuki and Lehane (2015a). As expected, the change in permeability does not change the magnitude of drained and undrained cone resistances.

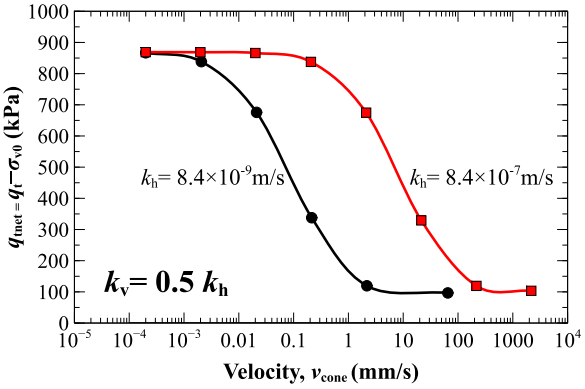

Figure 10. Effect of permeability on cone resistance dependence on velocity predicted by NorSand

5.4.4. Effect of initial state parameter (ψ_0)

The soil's current state, considered in the NorSand model by the initial state parameter, was investigated using three values, representing both loose (positive ψ_0) and dense (negative ψ_0) states. Fig. 11 illustrates the variations of cone resistance with penetration rate in soils having three different ψ_0 values but with all other soil parameters in Table 2 being the same.

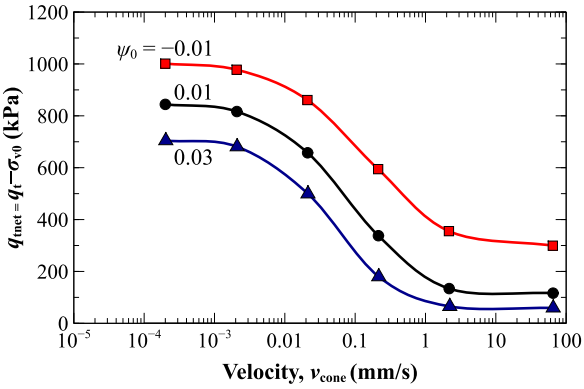

Figure 11. Effect of initial state parameter on cone resistance dependence on velocity predicted by NorSand

A clear pattern is evident where both drained and undrained resistances increase with reducing ψ_0. The overall curve moves upwards as the soil's state becomes denser while the ratio of drained to undrained cone resistance ($q_{tnet,drained}/q_{tnet,undrained}$) decreases as ψ_0 reduces. For example, the predicted $q_{tnet,drained}/q_{tnet,undrained}$ ratios for soil with ψ_0 = -0.01 and 0.03 are 3.3 and 12, respectively, demonstrating the significant importance of the state parameter.

5.4.5. Normalised velocity

Previous studies (e.g., Randolph and Hope (2004) and many others) suggest that drainage conditions during penetrometer tests depend on the probe diameter, penetration rate, and soil consolidation characteristics. CPT results of various probe sizes and penetration rates in different soil deposits can be represented by plotting normalised cone resistance ($Q = q_t - \sigma'_{v0}/\ \sigma_{v0}$) against normalised velocity (V) proposed by Lehane et al. (2009) below:

$$V = \frac{v \cdot d}{c_h} = \frac{v \cdot d \cdot \gamma_w \sqrt{\lambda \kappa}}{k_{h0}(1+e_0)\sigma_h'} \quad (5)$$

where v = cone velocity; d = cone diameter; c_h = horizontal coefficient of consolidation; γ_w = unit weight of water; λ = slope of critical state line in one-dimensional compression; κ = slope of unloading/reloading line in one-dimensional compression; e_0 = void ratio at in-situ vertical effective stress (σ'_v); and k_{h0} = horizontal permeability at this void ratio. This relationship was chosen particularly because it considers soil stiffness (represented in λ and κ) and effective stress level.

The net cone resistances obtained in section 5.4.1 were used and plotted against the normalised velocity. To identify the transition zone from drained to partially drained response or vice versa, Q/Q_D and Q/Q_{UD} were plotted against V in Fig. 12, where Q_D and Q_{UD} are normalised drained and undrained cone resistances, respectively. Fig. 12(a) shows that the partially drained conditions can exist at lower V values in soil with higher G/p_0'. For example, for a given V of 0.01, the penetration is almost fully drained in the soil with the lowest stiffness and partially drained in the other two stiffer soils; this same pattern is observed by Suzuki and Lehane (2015a).

Fig. 12(b) indicates that undrained conditions exist at lower V values in soil with higher G/p_0'; this contrasts with the results obtained by Suzuki and Lehane (2015a) using the HS model, where undrained conditions were found at $V \sim 30$. For comparison, the transition from partially drained to undrained conditions at V values of about 5 in the stiffest soils and 200 in the soil with the lowest stiffness. These results indicate that, contrary to assumptions made in general practice, the normalised cone resistance versus V curve is not unique, when the definition for V includes a stiffness or compressibility term (as is the case when c_h or c_v is used).

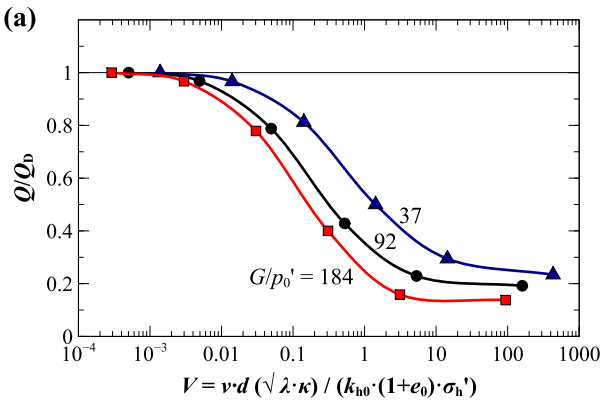

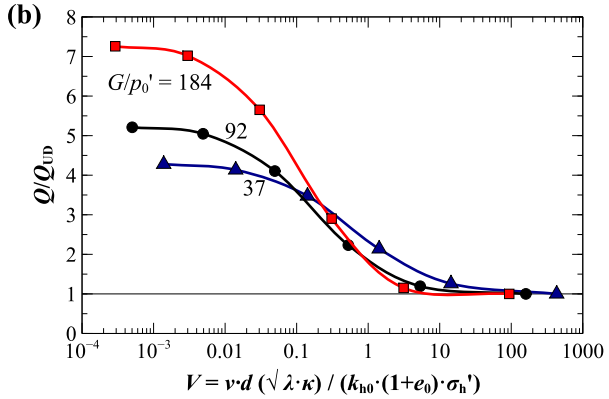

Figure 12. Q/Q_D and Q/Q_{UD} variations with normalised velocity (V) for soil with different stiffnesses

6. Conclusions

FE simulations of spherical cavity expansion adopting the NorSand constitutive model have been seen to provide good predictions of the variation of cone resistance with velocity for a sand-silt-clay mixture (SCS soil) and reasonable predictions for soil with 25% Kaolin and 75% sand.

Parametric analyses using NorSand show that the cone velocity at the transition between drained and partially-drained conditions, and between partially-drained and undrained conditions is independent of the soil stiffness. It follows that the use of the normalised velocity term currently used in practice cannot unify normalised cone resistance variations with penetrometer velocity for soils with widely varying stiffness.

Acknowledgements

The first author is grateful for the financial support from the UWA Graduate Research School (GRS) Travel Award and Lembaga Pengelola Dana Pendidikan (LPDP) of the Ministry of Finance of the Republic of Indonesia.

References

Bolton, M.D., Gui, M.W., Garnier, J., Corte, J.F., Bagge, G., Laue, J., and Renzi, R. 1999. "Centrifuge cone penetration tests in sand." Géotechnique, **49**(4): 543-552, https://doi.org/10.1680/geot.1999.49.4.543

Bentley Systems, Inc. 2022. PLAXIS 2D CONNECT Edition V. 22.02.00.1078, [Computer Program]. Bentley Systems, Inc.

Bentley Systems, Inc. 2022. *PLAXIS CONNECT Edition V22.00 User Defined Soil Models - NorSand: An elasto-plastic model for soil behaviour with static liquefaction*. Exton, PA: Bentley Systems, Inc.

Bentley Systems, Inc. 2023. *PLAXIS 2D 2023.2 Reference Manual 2D.2023*. Exton, PA: Bentley Systems, Inc.

Dienstmann, G., Schnaid, F., Maghous, S., and DeJong, J. 2018. "Piezocone Penetration Rate Effects in Transient Gold Tailings." J Geot Geoenv Eng, **144**(2): 04017116, https://doi.org/10.1061/(ASCE)GT.1943-5606.0001822

Jaeger, R.A., DeJong, J.T., Boulanger, R.W., Low, H.E., and Randolph, M.F. 2010. "Variable penetration rate CPT in an intermediate soil." In *International Symposium on Cone Penetration Testing (CPT '10)*, Huntington Beach, California.

Jefferies, M., and Been, K. 2015. *Soil liquefaction: a critical state approach*. 2 ed. CRC Press, London.

Jefferies, M.G., and Shuttle, D.A. 2005. "NorSand: Features, Calibration and Use." In *Soil Constitutive Models: Evaluation, Selection, and Calibration*, edited by J.A. Yamamuro and V.N. Kaliakin. American Society of Civil Engineers, Reston, VA. pp. 204-236.

Ladanyi, B., and Johnston, G. H. 1974. "Behavior of Circular Footings and Plate Anchors Embedded in Permafrost." Can Geot J, **11**(4), 531-553, https://doi.org/10.1139/t74-057

Lehane, B.M., O'Loughlin, C.D., Gaudin, C., and Randolph, M.F. 2009. "Rate effects on penetrometer resistance in kaolin." Géotechnique, **59**(1): 41-52, https://doi.org/10.1680/geot.2007.00072

Randolph, M.F., and Hope, S.N. 2004. "Effect of cone velocity on cone resistance and excess pore pressures." In *International Symposium on Engineering Practice and Performance of Soft Deposits*, edited by T. Matsui and Y. Tanaka and M. Mimura. Yodogawa Kogisha Co. Ltd, Osaka, Japan. pp. 147-152.

Reid, D., and Fourie, A. 2016. "Laboratory assessment of the effects of polymer treatment on geotechnical properties of low-plasticity soil slurry." Can Geot J, **53**(10): 1718-1730, https://doi.org/10.1139/cgj-2015-0343

Schanz, T., Vermeer, P.A., and Bonnier, P.G. 1999. "The hardening soil model: Formulation and verification." In *Beyond 2000 in Computational Geotechnics*. Routledge, https://doi.org/10.1201/9781315138206-27

Shuttle, D., Marinelli, F., Brasile, S., and Jefferies, M. 2022. "Validation of computational liquefaction for tailings: Tar Island slump." Geot Res, **9**(1): 32-55, https://doi.org/10.1680/jgere.21.00007

Silva, M. F. 2005. "Numerical and physical models of rate effects in soil penetration." PhD Thesis, University of Cambridge.

Suzuki, Y. 2015. "Investigation and interpretation of cone penetration rate effects." PhD Thesis, The University of Western Australia, Perth.

Suzuki, Y., and Lehane, B.M. 2015a. "Analysis of CPT end resistance at variable penetration rates using the spherical cavity expansion method in normally consolidated soils." Comp Geot, **69**: 141-152, https://doi.org/10.1016/j.compgeo.2015.04.019

Suzuki, Y., and Lehane, B.M. 2015b. "Cone penetration at variable rates in kaolin–sand mixtures." Int J Phy Model Geot, **15**(4): 209-219, https://doi.org/10.1680/ijpmg.14.00043

Vesić, A. S. 1972. "Expansion of Cavities in Infinite Soil Mass." J Soil Mech Found Div, **98**(3), 265-290, https://doi.org/10.1061/JSFEAQ.0001740

Vesić, A. S. 1977. "Design of pile foundations, National Cooperative Highway Research Program, Synthesis of Highway Practice No. 42." Transportation Research Board, National Research Council, Washington, D.C.

Yasufuku, N., and Hyde, A. F. L. 1995. "Pile end-bearing capacity in crushable sands." Géotechnique, **45**(4), 663-676, https://doi.org/10.1680/geot.1995.45.4.663